

Internal Lighting by Solar Collectors and Optical Fibres

P. Sansoni, D. Fontani, F. Francini, L. Mercatelli,
D. Jafrancesco and E. Sani, D. Ferruzzi
*CNR-INO National Institute of Optics, Largo E. Fermi, 6, 50125 Firenze,
Italy*

1. Introduction

Sunlight concentration on small surfaces is widely studied [1-3], experimented and mostly applied to photovoltaic power generation [4-6]. More rarely these solar collectors are coupled to optical fibres [7-9], with the advantage of always having a circular absorber shape. On the contrary the photovoltaic (PV) cell is typically squared and therefore it requires a secondary optical system to reshape the image and to improve the light distribution uniformity.

The introduction of optical concentrators, especially high concentration systems, has two positive effects: it reduces the area of expensive solar cells and it increases their efficiency. The main reasons for this development are enhanced efficiency of CPV (concentrating photovoltaic) systems due to new solar cells, improved size of PV installations and increasing interest in alternative technologies, both due to government incentives and to the poor Silicon availability. In general it can be assumed that an improvement in the volume of the collection system reduces the costs, given that the system provides a higher production of energy.

This chapter presents optical systems exploiting the sunlight using optical collectors and fibres to illuminate building interiors. In particular Sect. 5 describes in details a solar plant demonstrator installed to provide illumination of museum showcases [10]. This daytime lighting system was developed from design to production, installation and testing in working conditions. The light focused by the solar collector can be used either for direct illumination or to accumulate power [11] for lighting at times when there is no sunlight. The first function is obtained coupling an optical fibre to a solar collector. The second consists in focusing the solar light on a PV cell, which converts the light into electrical energy. This function has been suggested by the long closing times, typical of the museum. Due to the fact that the internal illumination was not required for hours or entire days (museum closure day), during these periods the PV cells can exploit the solar light.

A solar collector with optimised features and collection performance was specifically designed for mass production to reduce costs. The evolution of solar concentrators for fibre coupling [12-13] is discussed in Sections 2-3, with theoretical and experimental comparisons based on optical tests [14] performed on the realised samples. The field tests, with direct exposition to the sun, required to design and built suitable mechanical systems to support and move the concentrators: examples of tracking systems [15-16] are reported in Sect. 4.

Besides museum lighting required an alternative illumination source that can be used when sunlight is not available. This was realised by employing novel LEDs (Light Emitting Diodes) with very low power consumption. But several fundamental requirements must be met. First, illuminance levels are dictated by the need to control deterioration of the exhibit items. Moreover, the LED light must replicate light from the sun. Finally, light uniformity and colour are important. Light hue and colour balance were examined using photometric and colorimetric measurements [17-20] to define the suitable filters for plastic fibre and LED light. Additional tests were carried out on lens production to evaluate collection efficiency and image size, examine optical treatments and experiment the effects of external agents and UV exposure. Section 5 illustrates all mentioned aspects analysed during the development of the museum lighting plant.

2. Optical design of fibre-coupled collectors

Optical systems for sunlight exploitation have been optically designed and tested in our laboratory since 1997 [12-14, 10]. They are modular devices including solar collectors, optical fibres and mechanical and electronic systems for sun tracking. The main element of the device is the sunlight concentrator coupled to an optical fibre for power transportation to the utilisation point. Our first theoretical studies and practical experimentation of an optical system for sunlight collection were developed for a European project. The selected optical fibres were single fibres made of quartz, which are characterized by extremely reduced losses. The collector was optically designed to be coupled to an optical fibre with core diameter 0.6mm and numerical aperture $NA=0.48$ (angular semi-aperture 28.7°). Several optical projects, with increasing complexity, were designed for the concentrator and some of them were realized. The optical configurations included Mangin, Parabolic and Cassegrain collectors: Table 1 summarizes their main optical characteristics; in particular the last column reports the material chosen for the realisation.

| Label | Collector name | Primary mirror | Secondary mirror | Other optical elements | Material |
|-------|----------------------|----------------|------------------|---------------------------|-----------------|
| A1 | Standard Mangin | spherical | flat | | Glass |
| A2 | Modified Mangin I | spherical | spherical | | Glass |
| A3 | Modified Mangin II | spherical | spherical | correction lens | Glass |
| B1 | Parabolic | parabolic | flat | | Glass |
| B2 | Parabolic with lens | parabolic | flat | spherical correction lens | Aluminium |
| C1 | Conic Cassegrain CCM | elliptic | spherical | | Quartz, Plastic |

Table 1. Optical layouts of collectors coupled to quartz fibre $\varnothing=0.6\text{mm}$.

The efficiency obtained by each collector coupled to a 0.6mm quartz fibre was theoretically estimated and experimentally measured. This comparative study showed that the Cassegrain collector C1, especially designed for the European project, was the most compact and performed the best light collection. The Mangin configuration represented the best trade-off between collection efficiency and cost, since these collectors have only spherical surfaces that are easier to be optically manufactured. Concerning the mechanical alignment

between concentrators and optical fibre, for Mangin and Parabolic collectors this problem was more complex to solve than for the Cassegrain optics because they used a secondary mirror that is physically separated from the primary mirror (it is realized on the protective window). This alignment difficulty increased if an array of concentrators was used. Hence the modular unit was constituted by a tile mounting four collectors and each collector was coupled to a single quartz fibre.

Starting from the fibre-matching requirements of image diameter 0.6mm and $NA=0.48$, we developed the optical systems in Table 1. Then we estimated the illuminated area on the focal plane of each solar collector in order to compare the sun image to the fibre diameter. The image is mainly created by the spot within upper and lower rays, but it also includes the root mean square spot diagram at maximum field 0.25 deg (indicated in the following as "rms spot"). The rms spot size usually denotes the root mean square of the spot radial size and it gives information on the rays spread and thus on the geometrical aberration of the optical system. The diameter of this area should be within 0.6mm to obtain the best fibre-coupling.

Class A contains the solar collectors where all surfaces are spherical. These configurations present small image diameter and rms spot over 0.1mm. In class B there are systems with parabolic mirror, while the conic Cassegrain represents class C. Collectors of classes B and C are characterised by a very good image quality. These layouts are more complicated and expensive to be realised than the others, but in the best case the collected power is about three times higher with respect to A1. A3 is a trade-off between the two collector types since all its surfaces are spherical but the image quality is quite good. The enter pupil diameter of the solar collector varies from 40mm to 71mm and it has been optimised in the spectral range between 400nm and 1400nm of wavelength, for a 0.5 deg field of view. An exemplification of the images pertaining to the six optical systems under consideration is shown in Fig. 1. Within the fibre core (plotted as dashed circle) the central yellow spot indicates the sun image, while the two lateral dashed spots represent the rms spots.

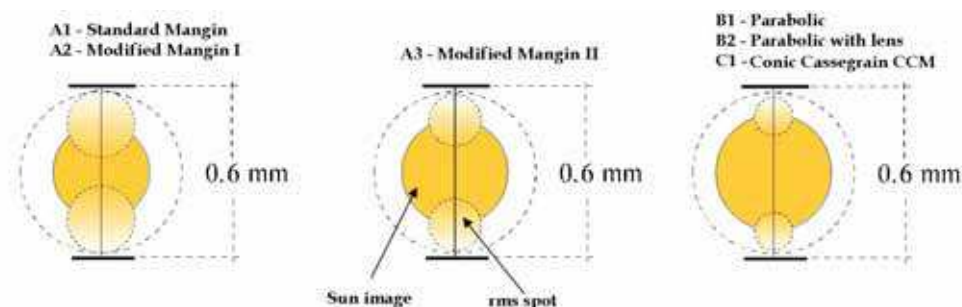


Fig. 1. Schematic view of images formed by the six collectors.

In the next paragraphs of this section each of the six optical layouts is described in details: optical configuration and performance are examined and compared. Then in Sect. 3 some experimental measurements on realised samples of the designed collectors are analysed and compared with the theoretical estimations.

2.1 Mangin collectors

The Mangin system is composed of a glass meniscus, aluminised on the rear surface, with a first spherical mirror and a secondary mirror, which can be flat or spherical. The optical path between the two surfaces of the meniscus allows the control of the spherical aberration, which can be minimised adjusting their curvature radius.

Three different configurations (A1, A2, A3) were selected, optimising their optical parameters with the aim of reaching the largest enter pupil diameter (EPD) in order to collect the maximum of power. The layouts are depicted in Figures 2, while the optical projects are reported in Figures 3: A1 in (a), A2 in (b), A3 in (c). All optical designs for A, B, C collectors were developed using Zemax ray tracing software.

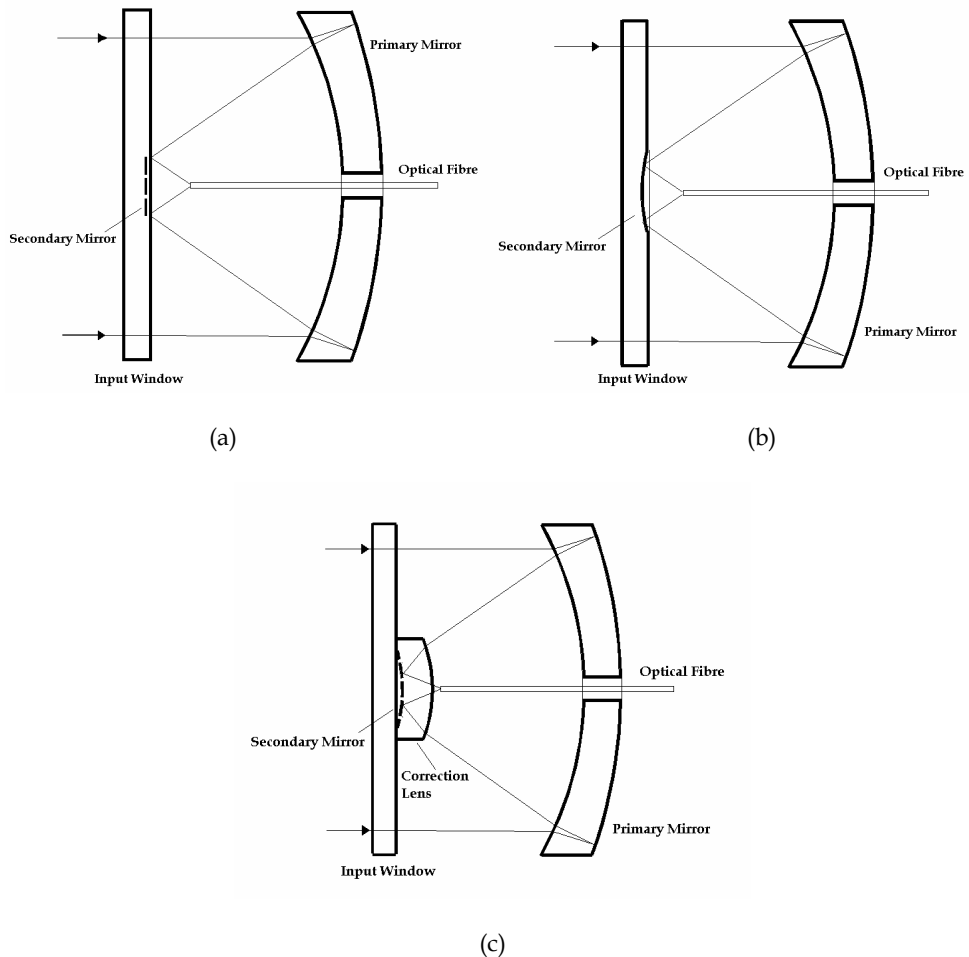


Fig. 2. (a) Layout of Mangin A1, (b) Layout of Mangin A2, (c) Layout of Mangin A3

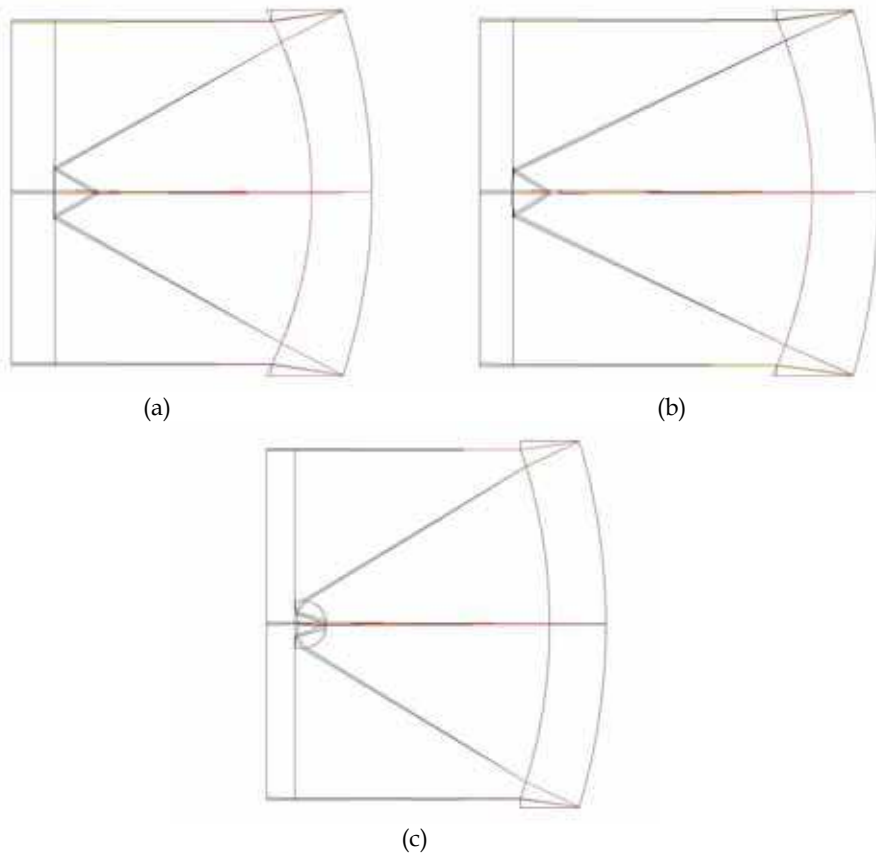


Fig. 3. (a) Zemax optical design of Mangin A1 (b) Zemax optical design of Mangin A2 (c) Zemax optical design of Mangin A3

They have the following optical features (the focal length f is at wavelength 580nm; $f/\# = f/EPD$ is the f number; θ is the maximum angle of rays with respect to the optical axis):

A1) spherical primary mirror; flat secondary mirror; maximum EPD=40mm; $f=39.76$ mm, $f/\#=0.994$ ($\theta=26.7^\circ$);

A2) spherical primary mirror; spherical secondary mirror; EPD=52mm, $f=48$ mm, $f/\#=0.923$ ($\theta=28.44^\circ$);

A3) spherical primary mirror; spherical secondary mirror with correction lens; EPD=62mm, $f=58.1$ mm, $f/\#=0.937$ ($\theta=28.5^\circ$).

Table 2 in Sect. 3.1 compares the main optical characteristics among all examined collectors of classes A, B, C.

Comparing the different layouts in class A, we can see that a more corrected system allows us to increase the enter pupil EPD and it yields to a higher collected power on the optical fibre. For A1 and A2 we can use Fused Silica to minimise the chromatic aberration; while for A3 we used SF1 glass for the primary mirror and PBM3 for the correction lens.

A1 is very cheap to realise, but the total spot diameter is small (0.513mm); while A2 allows to obtain a larger sun image (0.598mm). The total spot diameter for A3 is 0.594mm, but it is the most complicated: there is a correction lens on the surface of the secondary mirror (the rear surface of this lens was aluminised to avoid the crossing of two further surfaces). The differences among the sun images can be evidenced considering their profiles on a central line in the image plane. The curves for A1, A2 and A3 are reported in Fig. 4 plotting the average image profile versus the points along the image line.

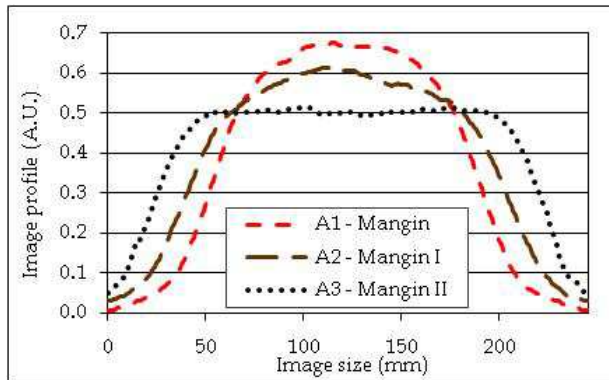


Fig. 4. Profiles of images for A1, A2, A3.

Standard Mangin A1 was realised in Glass in two versions: with EPD and f 40mm (Mangin40) or with EPD and f 60mm (Mangin60). The enlarged diameter of Mangin60 had the aim of improving the collected energy with respect to Mangin40. Modified Mangin A2 and A3 are more complicated to be realised, but the same performance level can be obtained by a standard Mangin of EPD 60mm. Thus Mangin60 represents a trade-off between A3 with EPD 62mm and A1. The manufacturing cost for the realisation of Mangin60 is low because of the traditional work to obtain spherical surfaces: a sample of Mangin60 is shown Fig. 5. For Mangin and Parabolic collectors the optical fibre is placed very close to the secondary mirror by means of a support crossing the collector in its central part, as Fig. 6 illustrates.



Fig. 5. Collector A1 (Mangin60) realized in glass.

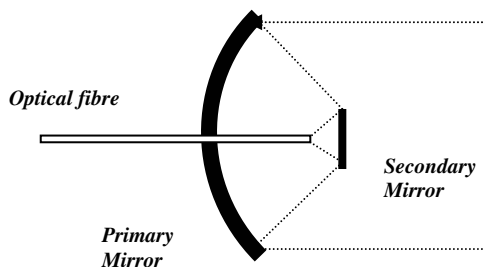


Fig. 6. Fibre position for Mangin and Parabolic collectors.

2.2 Parabolic collectors

The parabolic system is composed of two mirrors, the primary is parabolic and the secondary is flat, with or without correction lens: B1 and B2, respectively. The position of the secondary mirror is analogous of the corresponding Mangin layouts A1 and A3 shown in Figures 3a and 3c.

Figures 7a and 7b present the standard views of the optical designs for B1 and B2. To provide a more realistic view of B2, Fig. 7c presents a three-dimensional model of the Parabolic with lens.

The optical parameters are summarized in Tab. 2 of Sect. 3.1, but for B1 the maximum reachable EPD is 70mm, f is 65mm (at a wavelength of 580nm), $f/\#$ is 0.93 and the maximum axial angle θ is 28.3°; while for B2 EPD is 71.1mm, f is 65mm, $f/\#$ is 0.914 and $\theta=28.67^\circ$.

The optical quality of B1 is very good; the total spot diameter is 0.610 mm with a very high uniformity of light distribution, as shown by the image profiles in Fig. 8. It is useful to remind that a parabolic mirror is free from on-axis aberrations (spherical and chromatic), then the spot diagram for the on-axis field is exactly a point (if we do not consider higher order aberrations). In B2 an additional correction lens allows an improvement of the quality of this system, decreasing the off-axis aberrations (coma and astigmatism) and the total spot diameter results 0.598 mm. For B1 and B2 Fig. 8 compares the mean image profiles along a central image line. The figure evidences that the images of B1 and B2 are larger than those of the three Mangin collectors in Fig. 4.

B1 was realised by an Italian firm (SILO) as Glass parabolic mirror built by traditional optical working: EPD is 70mm and f is 65mm for the SILO parabolic mirror. A B2 sample was acquired among the commercial products available on the market, selecting the Aluminium Diamond turned parabolic mirror (by Advance - Coherent) with EPD=71.1mm and $f=65$ mm.

The useful features of the parabolic layouts are the optimised optical parameters, which create high collection efficiency, combined to a large enter pupil, giving a wide effective area. The output power, analysed in Sect. 3, depends on both efficiency factor and effective area. Collectors B1 and B2 represent the best solutions optimising these two quantities.

2.3 Conic Cassegrain collector

The optical project of the Catadioptric Concentrator Monoblock (CCM) was developed with the aim of optimising the optical characteristics of the collector but also its compactness. In Tables 1 and 2 it is classified as conic Cassegrain and indicated as C1. The first surface is elliptic and the second one is spherical. The maximum EPD is 56mm, f is 55mm and $f/\#$ is 0.98. As for the previous collectors, C1 fulfils the fibre-matching requirements: the output

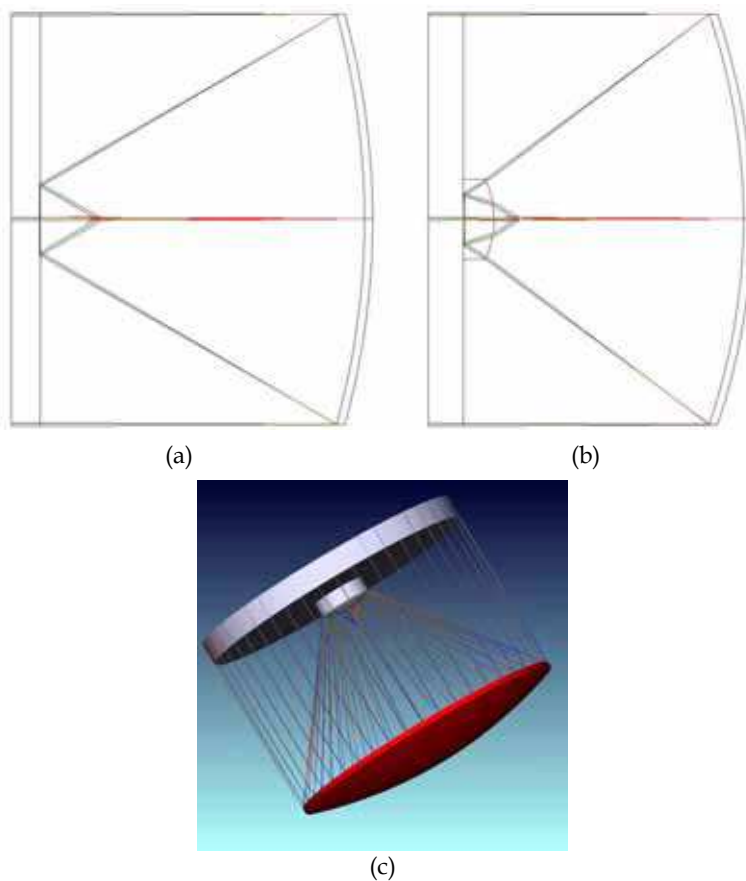


Fig. 7. (a) Zemax optical design of Parabolic B1. (b) Zemax optical design of Parabolic B2. (c) Zemax 3D model of Parabolic B2.

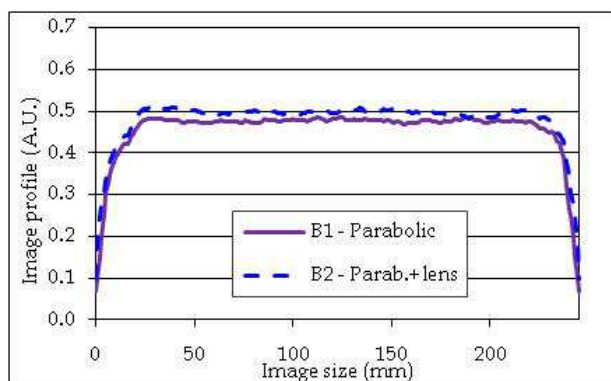


Fig. 8. Profiles of B1 and B2 images.

angle $\theta=26.98^\circ$ is within the fibre acceptance angle (28.7°) and the total image diameter (0.534mm) is considerably shorter than the fibre size (0.6mm).

The optical working principle of this collector is well known: it consists of two optical elements in a coaxial configuration of Cassegrain type. The C1 scheme is presented in Fig. 9; while Fig.10a reports the optical design and Fig.10b a 3D model. The characteristics of C1 seemed to be particularly useful for fibre-coupling and the realisation procedure appeared to be innovative.

C1 was realised in a unique piece of quartz (see Sect. 3.3), obtaining an objective characterised by extremely reduced dimensions and great mechanical stability. The input surface is flat and its central part was optically worked to obtain the spherical surface of the secondary mirror. The primary mirror is aspherical and in its centre there is a non-aluminised flat zone, which represents the output surface. The crossing of the glass constituting the concentrator along its entire internal optical path contributes to compensate the spherical aberration of the mirrors and it allows correcting the aberrations of a primary mirror with ellipsoid shape. The internal path within the material introduces acceptable chromatic aberrations.

Successively some samples of CCM were realised in PMMA ((polymethylmethacrylate), reducing weight and realisation costs (see Sect. 3.3).

The image profile of C1 is compared with those of B2 and A3 in Fig. 11 showing that the C1 image is larger than A3 (the largest Mangin image) but considerably smaller with respect to B2 (the largest Paraboloid image). The optical quality of this system is good, but lower with respect to the quality of the two parabolic ones (see Tab. 2 in Sect. 3.1).

The main advantages of C1 are immediately visible comparing the layouts of the six collectors, the CCM thickness (25mm) is considerably shorter and, being a monoblock, it is easier to be mounted and aligned. These characteristics of the CCM are a fundamental advantage since the device is modular and it is supposed to incorporate several collectors in each tile (illustrated in Sect. 4).

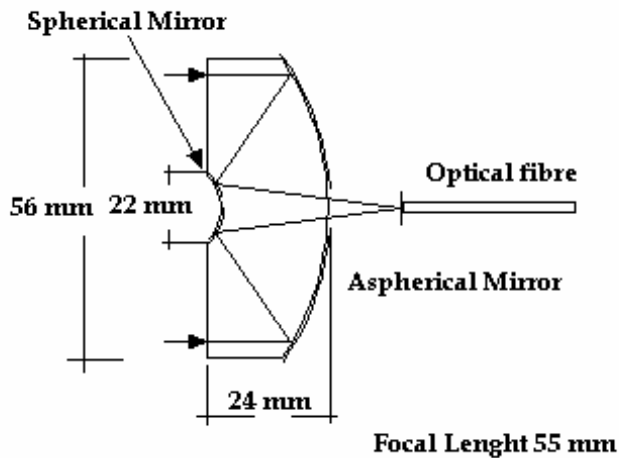


Fig. 9. Layout of CCM: collector C1.

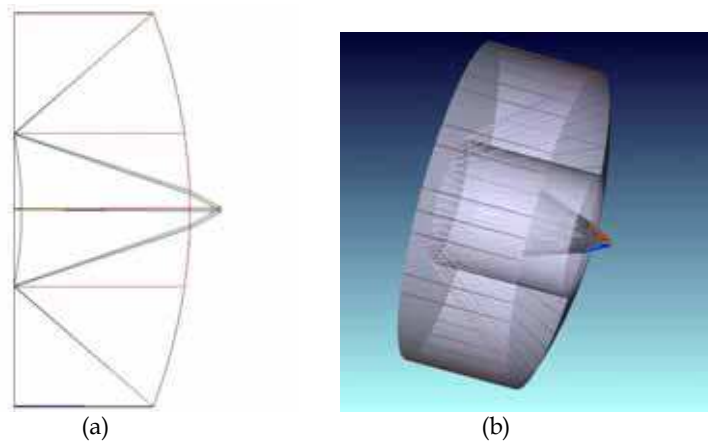


Fig. 10. (a) Zemax optical design of conic Cassegrain C1. (b) Zemax 3D model of conic Cassegrain C1.

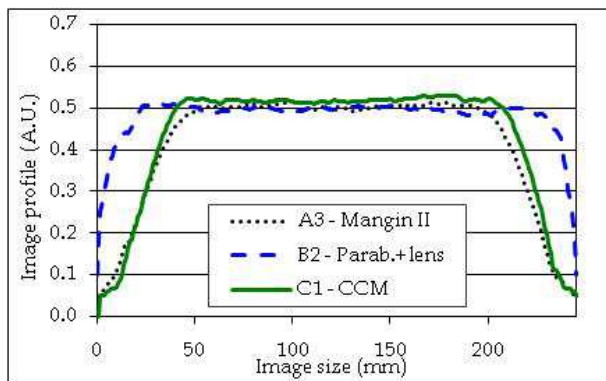


Fig. 11. Profile of C1 image, compared to B2 and A3 profiles.

3. Theoretical and experimental comparison of the collectors

3.1 Theoretical efficiency of collectors

Our modular device was composed of units, each of which consisted of a concentrator coupled to an optical fibre that transported the power to the utilisation point. Characteristics and performance of the six optical projects were theoretically estimated, calculating in particular the collection efficiency of each collector coupled to a 5m quartz fibre of size 0.6mm and $NA=0.48$. Table 2 summarises these optical features to compare the concentrators presented in Sect. 2.

Table 2 reports the power collection performance for the six concentrators of Tab. 1: the collector efficiency factor is the ratio output power / input power, while the total efficiency factor corresponds to the collector coupled to the fibre. The effective area is the surface effectively exposed to the sun and it was used to calculate the output power theoretically obtained at fibre end. In this output power calculation the total efficiency factor takes into

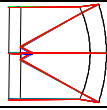
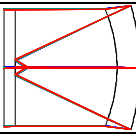
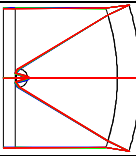
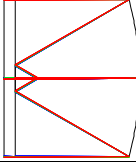
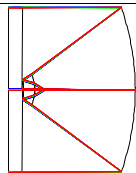
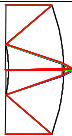
| 1 | 2 | 3 | 4 | 5 | 6 | 7 | 8 | 9 | 10 | 11 |
|---|-----------------------------|-------------------|------------|-----------------|---------------------|----------------------------|-----------------------------|-------------------------|-----------------------------------|------------------|
| Layout | Max. enter pupil diam. (mm) | Focal length (mm) | f/# number | Image size (mm) | Rms spot diam. (mm) | Total spot size (5+6) (mm) | Collector efficiency factor | Total efficiency factor | Effective area (mm ²) | Output power (W) |
| A1 - STANDARD MANGIN (M1 Spherical, M2 Flat) | | | | | | | | | | |
|  | 40.0 | 39.8 | 0.99 | 0.350 | 0.163 | 0.513 | 0.73 | 0.64 | 1230 | 0.677 |
| A2 - MODIFIED MANGIN I (M1 Spherical, M2 Spherical) | | | | | | | | | | |
|  | 52.0 | 48.0 | 0.923 | 0.418 | 0.180 | 0.598 | 0.73 | 0.64 | 2085 | 1.147 |
| A3 - MODIFIED MANGIN II (M1 Spherical, M2 Allum. Spher. Lens) | | | | | | | | | | |
|  | 62.0 | 58.1 | 0.937 | 0.500 | 0.094 | 0.594 | 0.66 | 0.58 | 3004 | 1.498 |
| B1 - PARABOLIC (M1 Parabolic, M2 Flat) | | | | | | | | | | |
|  | 70.0 | 65.0 | 0.93 | 0.567 | 0.043 | 0.610 | 0.81 | 0.71 | 3732 | 2.279 |
| B2 - PARABOLIC WITH LENS (M1 Parabolic, M2 Allum. Spher. Lens) | | | | | | | | | | |
|  | 71.1 | 65.0 | 0.914 | 0.560 | 0.038 | 0.598 | 0.73 | 0.64 | 3909 | 2.152 |
| C1 - CONIC CASSEGRAIN CCM (M1 Elliptic, M2 Spherical) | | | | | | | | | | |
|  | 56.0 | 55.0 | 0.98 | 0.480 | 0.054 | 0.534 | 0.73 | 0.64 | 2082 | 1.146 |

Table 2. Collectors characteristics and sunlight collection performance.

account all losses of the collector-fibre system. Data in Table 2 were evaluated considering the following efficiency factors: 0.9 per mirror surface, 0.95 per glass surface, 0.97 for the 5m quartz fibre. The effect of the protective glass that should cover the whole tile of collectors was not taken into account in this table. The input power density value considered was

860 W/m², which is approximately the solar irradiance arriving on the Earth surface in the best conditions at a latitudes around 45°N. While the standard value of the irradiance outside the atmosphere is 1367 W/m².

A crucial parameter in this comparative table is the estimation of the final power obtained at the end of the optical fibre coupled to each collector. The highest output power values correspond to the two Parabolic B1 and B2, followed by Mangin A3 power value. C1 and A2 reach output power levels slightly lower than Mangin A3, but they are still better than A1. Even though the C1 image appears to be as good as those of B1 and B2, the output power obtained by the CCM does not reach the parabolic values. The advantage of the parabolic optical projects is that they combine high collection efficiency with wide effective area: they optimise these two quantities maximising the output power. The most compact optical layout is C1 that allows obtaining high power concentration with reduced aberrations. Table 2 shows that the rms spot of aberrations (lateral dashed spot in Fig. 1) is significantly reduced for C1, B1 and B2, with respect to all Mangin collectors.

In conclusion if the main purpose is to maximise the output power the parabolic collectors will be preferred. The CCM will be chosen if we privilege the compactness and the facility to be mounted and aligned. By a commercial point of view, if the main requirement is to have a collector easy to be realised at a competitive price the Mangin collector will be the better solution. On the base of the optical projects described in Sect. 2 and compared in this section, samples of all collectors were practically realised. The results of their experimental tests are reported in the next section.

3.2 Experimental tests on realised samples

Several samples of concentrators in Tab. 1 were realised as discussed in Sect. 2 and we experimentally measured the performance of the realised collectors coupled to an optical fibre. The experimentation included laboratory tests and field measurements with direct explosion to the sun. The tests in laboratory were performed using an optical system reproducing the solar divergence [14]; while the field tests require the employment of tracking systems to correctly orient the concentrators (discussed in Sect. 4).

Only B1 of Tab. 2 was available as commercial product, while the other samples were optically manufactured by Italian firms on the base of the optical designs in Sect. 2. The results for the collection efficiency, which is the ratio between the power measured at fibre end and the power arriving on the collector effective area, are reported in Table 3. The experimental values were measured in Florence (Italy) during the month of November between 11.30 to 12.30 AM.

Taking into account efficiency results, realisation costs and optical system compactness, we decided to extensively test in real conditions only Mangin60 and CCM. Field tests were repeated in all seasons of the year and at different hours during the day. The average output power measured at the end of a 5m quartz fibre was 0.80±0.85 W for Mangin60 and 0.95±1.05 W for CCM in Silica. The CCM realised in PMMA (with EPD=56mm, $f=53.7$ mm and effective area 2082mm²) provided an output power of 0.80±0.90 W, thus resulting slightly less efficient than the CCM in Silica. For the plastic realisation of C1 the lower performance is both due to the use of PMMA instead of Silica (quartz) and to the more precise optical manufacturing of the Silica C1. Beyond the reduced thickness, easy mounting and easy aligning, the C1 in PMMA presents a further advantage: it is lighter and cheaper than C1 in Silica. The tests evidenced that the drawbacks of Silica C1 are heaviness and

| label | Collector | EPD(mm), f(mm), effective area (mm ²) | Theoretical efficiency at fibre end (Tab.2 col.9) | Lab. meas. of efficiency at fibre end | Field meas. of efficiency at fibre end |
|-------|----------------------------|---|---|---|--|
| A1 | Mangin 60 in Glass | 60.0, 60.0, 2672 | 0.64 | 0.41 | 0.33 |
| A1 | Mangin 40 in Glass | 40.0, 40.0, 1230 | 0.64 | 0.41 | --- |
| B1 | Paraboloid in Glass | 70.0, 65.0, 3732 | 0.71 | 0.39 | 0.31 |
| B2 | Paraboloid (commercial) | 71.1, 65.0, 3909 | 0.64 | 0.32 | 0.33 |
| C1 | CCM in Quartz | 56.0, 55.0, 2082 | 0.64 | 0.54 | 0.53 |

Table 3. Experimental efficiency of sunlight collection.

difficulties to realise the aspherical surface and obviously the very high cost for this realisation. The CCM in PMMA reduces both weight and costs still providing good collection efficiency.

It is useful to note that the obtained output power is in sunlight, whose luminous efficacy is much higher than that of electric lighting. The luminous efficacy is 70÷105 lm/W for direct sunlight and 110÷130 lm/W for diffuse skylight [21]; while for an incandescent lamp it is 10÷18 lm/W [22]. Hence the application to internal illumination exploits also the elevated luminous efficacy of solar light.

3.3 Plastic collector development

The successive step was the development of plastic optical components, which reduced the realization costs. Collector C1 was realized both in Silica (quartz) and in PMMA (plastic); it is important to note that the optical project of C1 ought to be redesigned for the realization

| 1 | 2 | 3 | 4 | 5 | 6 | 7 | 8 | 9 | 10 | 11 |
|-------------------------------------|-----------------------------------|-------------------------|---------------|-----------------------|------------------------------|----------------------------------|-----------------------------------|-------------------------------|---|------------------------|
| Layout and realisation | Max. enter pupil diam. (mm) | Focal length (mm) | f/# number | Image size (mm) | Rms spot diam. (mm) | Total spot size (5+6) (mm) | Collector efficiency factor | Total efficiency factor | Effective area (mm ²) | Output power (W) |
| <i>C1 in Fused Silica</i> | <i>56.0</i> | <i>55.0</i> | <i>0.98</i> | <i>0.480</i> | <i>0.054</i> | <i>0.534</i> | <i>0.73</i> | <i>0.64</i> | <i>2082</i> | <i>1.15</i> |
| C1 realised in Quartz | 56.0 | 55 | 0.98 | --- | --- | 0.8 | 0.66 | 0.54 | 2082 | 0.97 |
| <i>C2 in PMMA (plastic)</i> | <i>56.0</i> | <i>53.7</i> | <i>0.96</i> | <i>0.5</i> | <i>0.075</i> | <i>0.075</i> | <i>0.73</i> | <i>0.64</i> | <i>2082</i> | <i>1.10</i> |
| C2 realised in PMMA | 56.0 | 54 | 0.96 | --- | --- | --- | --- | --- | 2082 | 0.85 |

Table 4. Features and collection performance of Cassegrain CCM collectors.

in PMMA (polymethylmethacrylate). Table 4 summarises optical parameters and collection performance of conic Cassegrain CCM collectors: it compares two theoretical optical projects, C1 in Fused Silica and C2 in PMMA (*in italics*), to the CCM manufactured in quartz and plastic. The measurements on C1 realised in quartz were performed in laboratory and inside a hole of 0.6mm diameter there was 84% of the total energy in the focal plane. The output power for C2 realised in PMMA is the average of the values obtained in the field tests.

Two CCM samples are presented in Fig. 14: Fig. 14a shows a C1 in Silica, Fig. 14b a C2 in PMMA. The optical performance of the two components was comparable, but the weight was considerably reduced for the plastic optics. The work proceeded modifying the optical project of collector C2 for being mass produced and for being coupled to a larger optical fibre (with core diameter 1.2mm and $NA=0.48$). The final component was an aspherical lens in PMMA (described in Sect. 5.1) with much reduced width (14.9mm) and weight (24g) compared to the C1 in quartz (width 23.8mm, weight 136g).

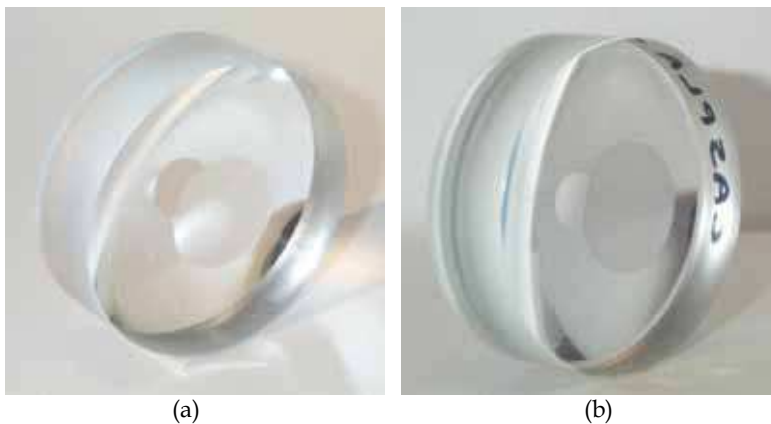


Fig. 14. (a) Cassegrain collector C1 realized in quartz. (b) Cassegrain collector C2 realized in plastic.

A further improvement was the use of plastic (or glass) fibre bundles instead of quartz single fibres. Considering the coupling to the aspherical lens in PMMA, the chosen value for the core diameter of the single fibre was 1.5mm, to take into account the spot enlargement and to facilitate the alignment. For the museum application to the illumination of several very large showcases (3m X 5m), requiring a large number of lighting terminations, fibre bundles were preferred. Optical fibre bundles made in plastic are very flexible, almost unbreakable and considerably cheaper than quartz fibre bundles, especially for a diameter of 1.5mm. Moreover for such a large core diameter a plastic fibre has extremely shorter bend radius with respect to a quartz fibre (as discussed in Sect. 5.4).

4. Sun tracking systems to support and orient the collectors

4.1 Sun tracking method

The sun tracking technique was studied [15], experimented and tested under working conditions. Suitable mechanical systems, to support and move the optical system, were

designed and built. The movements to align the optical collectors in the sun direction were performed in two directions by using an equatorial configuration: the directions being on the temporal axis and on the declination axis.

The methodology to track the sun position employed a double guiding system that uses two complementary procedures. The first one provides the preliminary orientation, then the second realises the fine positioning and adjustments. The first tracking system is of a passive type and drives the motors to correctly orient the collectors every day of the year. The second one is of a dynamic type and employs an optical pointing system. The core of this active tracking system is the sun pointer, which works as a double pinhole camera [16]. The pointer has two sensors, with decreasing field of view, that are used in sequence, improving the precision of the sun tracking. The system tracks the sun position with an angular precision higher than 0.1° . It is reliable and adaptable to all weather conditions and environmental variations. In the case of sun shading or temporary sun absence, the system provides a realignment of collectors in a few seconds. Furthermore, it is able to compensate for possible errors in the positioning of the device, which should be placed with the temporal axis parallel to the Earth's axis.

The solar collecting device is modular and its basic unit is a tile holding four concentrators. The tiles are mounted on a support whose orientation follows the sun position using a tracking system. This modular solar plant can be placed either on the roof or in the playground of a building.

4.2 The tile with 4 Mangins and 4 Cassegrains

Mangin and CCM Cassegrain concentrators were mounted on tiles of four collectors, as shown in Fig. 12a and 12b, respectively. The use of a small tile facilitates the alignment operations and improves the possibility of its massive reproduction, so the tile dimensions were 14cm x 14cm. Reduced size of the tile and system geometry makes it adaptable to the available space and to specific architectural requirements.

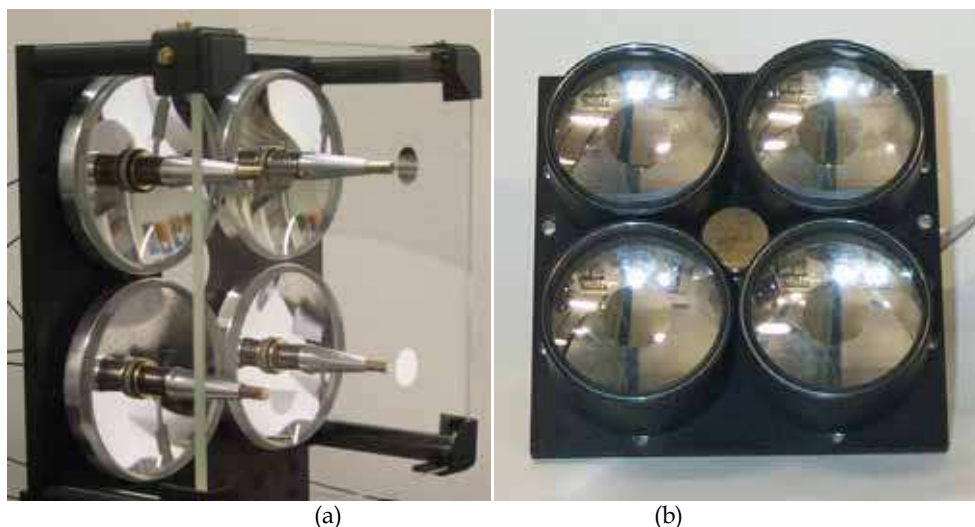


Fig. 12. (a) Tile of 4 Mangins.(b) Tile of 4 CCM Cassegrains.

Fig. 12a presents the tile with 4 Mangin60 collectors made of glass. The housing for the single collector is a metallic support of diameter 64 mm, which also holds the mirror. The fibre holder with its focusing adjustment is placed in the centre of the metallic support. The secondary mirrors are realised by evaporated aluminium on the input window covering the four collectors; consequently the Mangin alignment is more difficult than for CCM.

The tile holding 4 CCM collectors made of quartz is shown in Fig. 12b. The fibre adjustments mechanism is placed in the rear part of the tile, behind the collector. The sensor driving the sun tracking system is visible in the centre of the tile in Fig 12b.

Both tiles had the same external dimensions, so they were exchangeable if they were mounted inside the same moving support.

4.3 Motorised frames holding 1 tile or 9 tiles

Suitable mechanical and electronic systems were developed to support and move the optics. The equatorial structure included two motors, one for the temporal axis and one for the declination axis. Optical collector movement was performed by a double guiding system: preliminary orientation by a passive system driving the motors to correctly orient the optics on a daily basis, then fine positioning and adjustments using an optical sun pointer. These electro-mechanical structures were necessary to perform field test, with direct exposition to the sun of the collectors. To test in operative conditions the realised collectors, two different moving frames were realised. The first (Frame A) supported a single tile of four collectors: in Fig. 13a it mounts Cassegrain C1 collectors. It includes the sun tracking system and two micro motors, which keep the tile aligned in the sun light direction. The second configuration (Frame B) contained 9 tiles in a larger frame that can contain 36 collectors: Fig. 13b shows the frame with Mangin collectors. The dimensions are for Frame A: 16cm x 24cm; and for Frame B: 60cm x 60cm. The tiles in Fig. 12a and in Fig. 12b are interchangeable, so they can be mounted on both frames.

The most interesting feature of these frames is their self-alignment capability.



(a)



(b)

Fig. 13. (a) Frame A testing C1 collectors. (b) Frame B testing Mangin A1 collectors.

5. The application to internal museum illumination

The possible applications of this innovative solar device were room illumination, water heating or energy supply for domestic devices. For this latter use a photovoltaic panel provides the conversion into electric energy, which can be stored for later use. However the most promising application of these systems appeared to be the illumination of buildings, in particular for artistic purposes such as in museums or in special uses requiring solar light (colour rendering and colour recognition). In these cases the low power level reached by the system is an advantage, because the lighting of artworks has illuminance restrictions for their conservation. On the other hand direct solar lighting has an additional value in museum exhibitions, since it improves the colour rendering of the exposed objects, and it is necessary for colour identification in industrial production, which is fundamental for example for fabric. Hence our original system for sunlight collection was applied to internal lighting and in particular it was adapted to illuminate museum interiors [10]. It was developed from optical and electro-mechanical design to production, installation and testing in working conditions. The device included solar collectors, optical fibres, photovoltaic cells, mechanical and electronic systems for sun tracking. The optical collector was studied with comparative ray tracing analyses and experimental tests to optimise the optical configuration. Then the optical design was adapted to plastic component production to reduce costs. The final concentrator was a narrow and lightweight aspherical lens made of plastic. To provide illumination, the solar collector is coupled to a fibre bundle. For energy supply the sunlight is concentrated on a photovoltaic cell that converts the light into electric energy for utilization or storage. In addition the museum required an alternative light source for the case of sun absence, which was realised by low power consumption LEDs (Light Emitting Diodes).

A plant demonstrator was successfully installed in a Florentine museum, where it was developed and adjusted to illuminate the interior of large showcases with front size of length 5m and height 3m. Figure 14 presents a solar collecting device of the museum plant. The installation consisted in two groups of devices placed in two separated locations: on the museum roof, shown in Fig. 15a, and on the museum garden, shown in Fig. 15b.

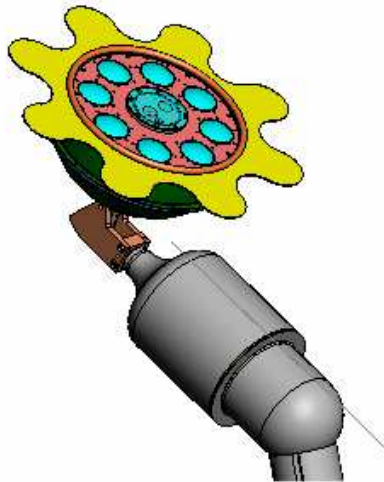


Fig. 14. A device of the museum plant demonstrator.

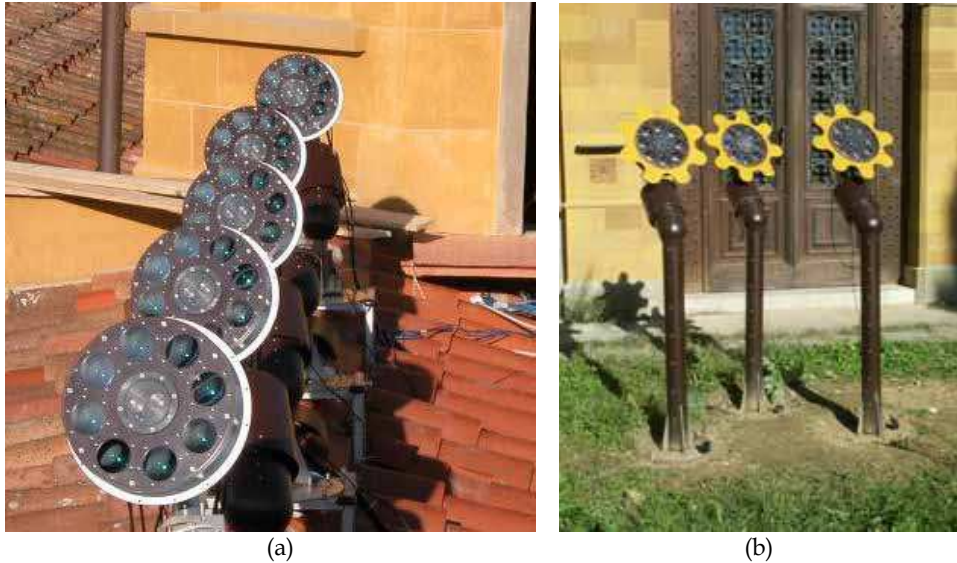


Fig. 15. (a) The installation on the museum roof. (b) The installation on the museum garden.

Collector samples were tested to assess collection performance; they also endured optical tests in operative conditions. Plastic and glass fibres were preferred to quartz fibres due to the difficulties of museum installation. Therefore the long fibre bundles represented the main cause of energetic losses, but some light can also be lost in an imprecise collector-fibre coupling. Fibre bundles transported the light inside the showcases realizing the lighting points, which were suitably distributed to maximize illumination uniformity. Appropriate filters, selected to achieve colour balance, were mounted on plastic fibre and LEDs. The museum experts indicated the correct illuminance levels, taking into account the recommendations of the International Council of Museum [19] for the exposed objects: they were basically weapons, armatures and metallic objects; the more fragile exhibit items were costumes and textiles. The result was a quite uniform lighting separately obtained by optical fibres or LEDs: both illuminations fulfilled illuminance equivalence and illuminance level requirements.

5.1 Collectors and fibres for the museum plant

For more than a decade our laboratory has studied sunlight collectors comparing the optical performance of different configurations to concentrate sunlight into an optical fibre [12-14]. Collection efficiency assessment and optical characterisation were carried out on samples of Paraboloids, Mangin collectors and a specially designed concentrator called Catadioptric Concentrator Monoblock (CCM). The Cassegrain collector CCM, presented in Sect. 2.3, was realised in quartz (Silica) and in plastic (polymethylmethacrylate PMMA): the plastic version has considerably reduced dimension, weight and cost, maintaining good collection efficiency.

Finally, to obtain the collector for the museum demonstrator, the optical project of the plastic CCM was adapted to provide collectors that could be mass produced, so allowing a significant reduction in cost. The result was a narrow and lightweight aspherical lens made

of PMMA: Fig. 16 shows a sample. Figure 17 compares the optical project of the aspherical lens in PMMA, designed for coupling with a plastic fibre of core diameter 1.2mm, to the optical project of the Conic Cassegrain in PMMA (collector C2), designed for coupling to a quartz fibre of core diameter 0.6mm. The comparison evidences that the main effects of the adaptation of the optical design were to simplify the optical surfaces and to lengthen the focal distance. In the optical design of the plastic aspherical lens the focal distance is 54.5mm, the entrance pupil diameter is 55mm, the numerical aperture is 0.48 and the thickness is 14.9mm.

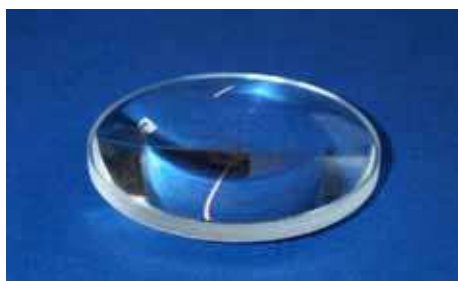


Fig. 16. A sample of the production of aspherical lenses in PMMA.

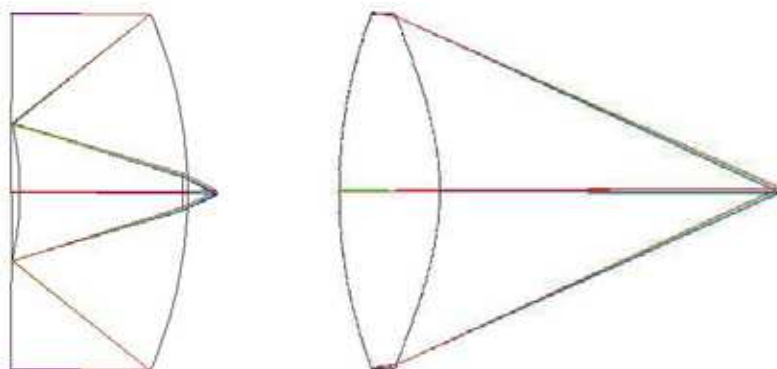


Fig. 17. Comparison of the optical designs: Cassegrain in PMMA (left) and aspherical lens in PMMA (right).

A first production of this plastic collector was realised for the museum installation. Tests were carried out on lens production to evaluate collection efficiency and image size (in Sect. 5.2), examine optical treatments and experiment the effects of external agents and UV exposure (in Sect. 5.3). The optical parameters, measured on randomly selected samples, presented extremely reduced standard deviations, confirming production homogeneity and reproducibility of lens fabrication process.

To enhance the collection efficiency the lenses had an anti-reflection treatment on both sides: the tests, repeated on the treated lenses, verified the expected performance improvement. The average collection efficiency E of the coated lenses was 98% and in addition the treatment reduced the E standard deviation. The features experimentally measured on the production samples were: mean focal length of 62.4mm, diameter of 55mm and width of 14.9mm.

The lenses were exposed to the external atmospheric agents to test the endurance of the treatment; then to simulate the operative conditions, the samples experienced an artificial Ultra-Violet irradiation, using a UV lamp. The most disturbing effect was water condensation, basically due to humidity and thermal excursion; while the effect of UV exposure was negligible on the lens spectrum. So the anti-reflection treatment lasted on the lenses, which maintained a very high optical quality with more than 95% of collection efficiency.

Each solar lens was coupled to a polymeric fibre bundle of length 30m, which had seven terminations, at its other extreme, arriving into the showcases. These terminations were optical fibres of core diameter 1.5mm and $NA=0.48$: they represented the actual lighting points, suitably arranged within the museum showcases, as discussed in Sect. 5.6. Fibre bundles were preferred to single fibre because the higher number of terminations allows illuminating the large showcases with more uniformly distributed light. The number of optical fibres in a bundle is defined by the circular geometry necessary to realise the bundle: 7 is the first possible fibre number after 1. Optical features of plastic and glass fibres are compared in Sect. 5.4, where the choice of plastic fibres is justified. For the specific application of museum lighting experts in this area suggested the use yellow-orange light: this aspect is discussed in Sect. 5.5.

5.2 Light collection and image size of the plastic lens

Sunlight collection efficiency was assessed on twenty samples of plastic collector production, randomly selected from available lenses. The optical tests were performed on a white light collimator, which reproduced the solar light divergence, examining collection efficiency E and focal distance f . The efficiency of sunlight collection [14] is measured as a ratio between the light focused within the nominal image and the light entering in the lens EPD (enter pupil diameter). The nominal image of the lens is the image obtained from a ray tracing simulation using the optical project of the lens: it had approximate diameter 1.2mm. The E values are obtained with a possible error of $\pm 2\%$. The tests were addressed to verify the homogeneity of the plastic lens production and reproducibility of the lens fabrication process. The average focal length was 62.4mm with a standard deviation of 0.28mm.

The plastic lenses were treated on both faces with an anti-reflection coating to improve efficiency of sunlight collection. Measurements of f and E were repeated on the treated lenses and test results confirmed the expected improvement in collection efficiency values. The treated lenses reached an E value of 99%, with an average value of 98%; while the lenses without treatment reached 93%, with a mean value of 91%. But the more interesting result is that the anti-reflection treatment reduces the standard deviation of the E data from 1.3 to 0.58.

For focalization into a fibre it is useful to measure image spot dimension and light distribution within the focused image. The optical set-up for this image control included a white light source reproducing the solar divergence. The beam impinged on the tested lens and a detection system was located in its image plane. It consisted of a photo-detector combined with a multi-hole mask, with hole diameters \varnothing from 0.8 mm to 1.6 mm. Each hole of the mask acted as a spatial filter on the image. The mask was moved in front of the detector to measure the light corresponding to each hole. The light was measured by the current generated by the detector. The data for filtered images were compared to the data for unfiltered image. The results of filtered image light were relative measurements, expressed as a ratio with respect to the total light flux in the focal plane.

This image analysis verified that the lens production was homogeneous in this aspect. The filtered image light, expressed as a percentage, was: 95% ($\varnothing = 1.2\text{mm}$); 98% ($\varnothing = 1.3\text{mm}$);

99% ($\varnothing = 1.5\text{mm}$). The diameter 1.2mm corresponds to the nominal image of the PMMA lens. While the value 1.5mm corresponds to the core diameter of the optical fibre selected for the museum plant.

5.3 Plastic lens exposure to atmospheric agents and UV irradiation

The solar lens with anti-reflection coating was tested in various atmospheric conditions to estimate the endurance of the treatment. An obvious negative effect was the deposit of raindrops or dust on the upper lens surface. However, the most disturbing effect appeared to be water condensation on the lower lens surface, occurring in sunny weather or raining conditions, because it is basically due to moisture presence and thermal changes between night and day. The collection efficiency E was monitored during the first ten weeks of exposure to the atmosphere. E was measured every week before and after cleaning the lens, since there were water droplets on one or both lens surfaces. Without cleaning, E decreased from 97% to 93% in three weeks, then E fluctuated between 91% and 76%, with an average value of 83%. The measurements on the lens covered by droplets and moisture had very low reproducibility and reliability. The results for cleaned lenses showed a very slight decreasing trend during the ten testing weeks, with E going from 97% to 95%.

Another essential analysis for the anti-reflection treated lenses is the exposure to ultra-violet radiation. The plastic used to manufacture the lenses is PMMA (polymethylmethacrylate) and UV irradiation typically induces a colour variation from transparent to yellow in this material. The anti-reflection treatment on the PMMA lens should reduce this degradation effect. A test was performed with a continuous exposure to an UV lamp for several weeks. It was found by measuring lamp and sun emissions with the same power meter in the same spectral range that UV laboratory radiation corresponds to about three months of sunlight exposure. The measurements did not show evidence of colour variations in the plastic lens material: comparison of the spectral transmission (in the wavelength range 200nm to 700nm) measured before and after UV irradiation indicated the difference was within the experimental error of the spectrometer.

In conclusion the collection efficiency of coated lenses was mostly affected by moisture presence and thermal changes between night and day. However these are only test examples and preliminary analyses, aimed at estimating how the operating conditions affect the solar collector efficiency. It would be useful to perform more detailed tests to correlate each single element (temperature, moisture, cloud cover amount, wind speed, spectral range of the radiation, etc) to the deterioration of performance of the plastic lens.

5.4 Fibre selection and tests for the museum installation

The optical coupling between solar lens and fibre bundle was one of the major causes of energy losses in the whole optical system of the museum demonstrator. The focused light should be received by the fibre with the maximum optical coupling obtained in the best alignment condition. As regards the core diameter, we finally chose the value of 1.5mm, to take into account the spot enlargement and to facilitate the alignment.

Another important cause of losses was the absorption in the optical fibre, which basically depends on material, diameter and length of the fibre. The fibre bundles should be characterised by high performance as regards spectral transmission. Typical materials for optical fibre production are quartz, glass and plastic. Silica has very good light transmission, but it is expensive, especially for bundle production, and quartz fibres are very fragile and

rigid. Glass fibres have a light attenuation higher than silica fibres, but they are considerably cheaper and more flexible, which is a fundamental advantage. Generally plastic is the preferred material to make fibres bundles, since it facilitates production and plastic fibre bundles are inexpensive, almost unbreakable and extremely flexible. In particular they have a bend radius of few centimetres for a fibre diameter of 1.5mm, while a silica fibre of the same diameter has a 900mm bend radius. Glass fibres are slightly more rigid than plastic ones, but they usually have lower transmission losses. Nevertheless an innovative plastic fibre bundle, realised in a polymeric mixture with an original composition, can reach a similar transmission performance to that of glass fibres.

For the museum installation, fibre bundles were selected in preference to a single fibre. Two fibre materials, glass and plastic, were considered by examining samples of fibre bundle with seven terminations: our samples of plastic fibres were produced by DGA (www.dga.it), while the samples of glass fibres were produced by 3M (www.3m.com). The sample of plastic fibre bundle had a single core diameter of 1.5mm and length 30m. The sample of the glass fibre bundle had a single core diameter 0.6mm and length 40m. To compare the optical performance of these two fibre types, measurements were carried out with sunlight and by analysing the illuminance at the fibre ends. These field tests examined the light transmitted by the seven terminations of the fibre bundle coupled to the plastic lens exposed to the sun. The use of the sun tracking system (in Sect. 4) is fundamental for performing these tests, because it keeps the lens in the sun's direction. The tests were performed at noontime, when the illuminance of the sunlight impinging on the demonstrator collectors was 950 lx to 1020 lx. Measurements were repeated with various sun conditions and on different days.

The illuminance obtained on the exposed object was measured at two reference distances: 50cm and 75cm. These lengths correspond to minimum and maximum distances between lighting points and exposed objects within the museum showcases. For the plastic fibre bundle the illuminance was 300 lx to 510 lx at 50cm and 150 lx to 270 lx at 75cm. The glass fibre bundle provides illuminance values of 340 lx to 560 lx at 50cm and 230 lx to 260 lx at 75cm. As seen from the results, the measurement values fluctuate during the test and it was found that they can vary even more between days and sun conditions. The final choice for the application of the museum plant was to employ polymeric fibre bundles.

5.5 Light level and colour suitable for museum illumination

The museum demonstrator employed a combination of solar light and other sources, represented by white LED with high emission levels at low supplying power (DGA product number 700001.31 "1W fixed LED gem", ref. www.dga.it). Museum object illumination has specific requirements on illuminance levels, light colour and light distribution uniformity. The first task was to reach a mean illuminance of 100÷120 lx, with the uniformity of light distribution being maximised within the showcases. The second task was the colorimetric equivalence between LED and fibre illumination. The third task was to obtain a yellow-orange colour. This section is devoted to photometric analyses and colour studies on the three light categories: sunlight guided by glass and plastic fibres and LED emission. The purpose was to minimise the colour difference between the three illumination categories by introducing suitable filters. The aspect of illuminance values is separately examined in Sect. 5.6, since they depend on the source distribution within the showcases.

A preliminary analysis compared the spectral components of the three illumination categories. Figure 18 presents the emission spectrum of the white LED and the illuminance spectrum of the sun after passing through glass and plastic, in the visible range. They were

measured using a Minolta CS1000 spectrophotometer, which examined a *Spectralon* (LabSphere™) surface illuminated by the radiation under test. The LED light was located between 420nm and 700nm and it was characterised by two isolated peaks, while the light guided by fibres presented a more continuous spectrum. Glass fibres transmitted in the whole visible range and over 800nm in the infra red region. The transmission of plastic fibres lied within 380nm and 700nm, almost covering the whole visible range. The colour temperatures were 4294 °K for glass fibres, 7982 °K for plastic fibres and 5183 °K for the white LED, whilst the Colour Rendering Index was: 95.4 for glass fibres, 67.3 for plastic fibres and 72.8 for the LED. A visual comparison of the solar illumination transmitted by the two fibre types is shown in the photo of Fig. 19: plastic fibres supplied a blue illumination, while glass fibres provided a yellow lighting.

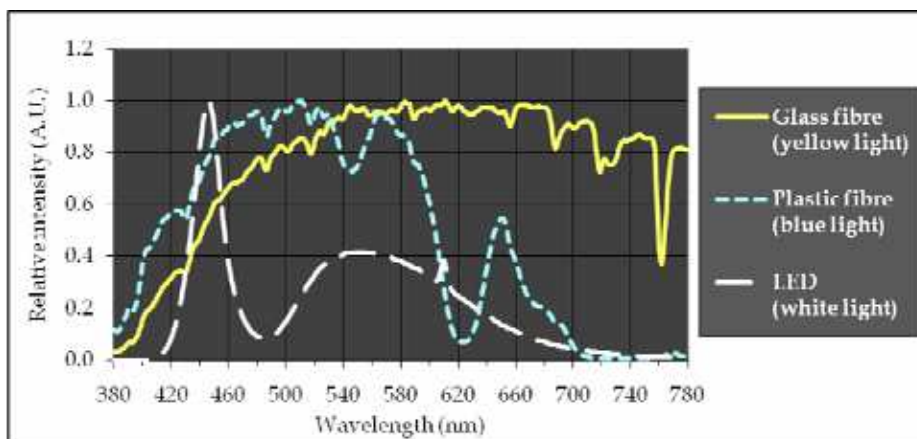


Fig. 18. Spectral comparison of the lighting using white LED, plastic and glass fibres.

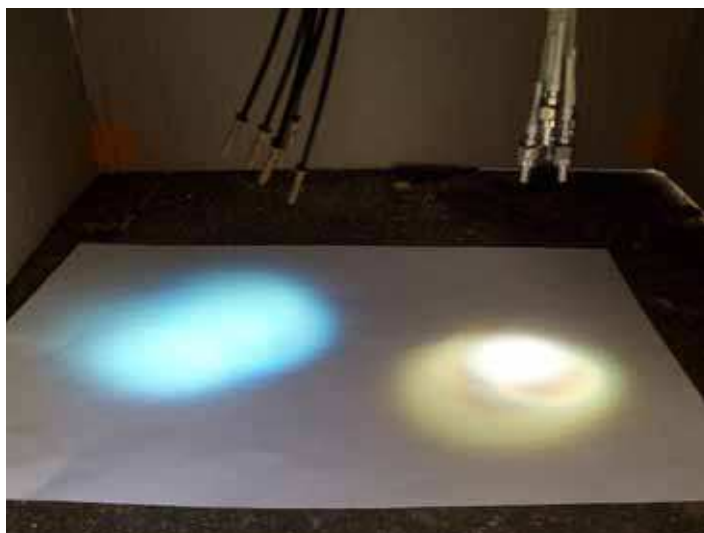


Fig. 19. Visual comparison of the sunlight transmitted by plastic and glass fibres.

Glass fibre appeared to be more appropriate for obtaining the correct hue. Nevertheless for the museum installation we finally decided to use polymeric fibre bundles because they are almost unbreakable and easier for installation, owing to their very short bend radius. However, the light guided by polymeric fibre bundles required some filtering.

The introduction of filters was necessary to match colour requirements. The filters were chosen from the catalogue of *Supergel filters* produced by Rosco (www.rosco.com). The museum experts preferred the yellow hue of the light transmitted by glass fibres to the blue hue of the plastic fibre illumination. Therefore, the glass fibre light was taken as the reference for the colour matching, and filtering was used for the other two lighting categories. In addition to modifying the colour, the filter attenuated the light, thus reducing the illuminance obtained within the showcases.

The selection of suitable filters was performed on the basis of photometric tests between the three lighting categories. The scheme for Colour_Test_1, comparing Glass Fibre and LED lights, is reported in Fig. 20a; while Fig. 20b presents the scheme for Colour_Test_2, comparing Plastic Fibre and filtered LED lights.

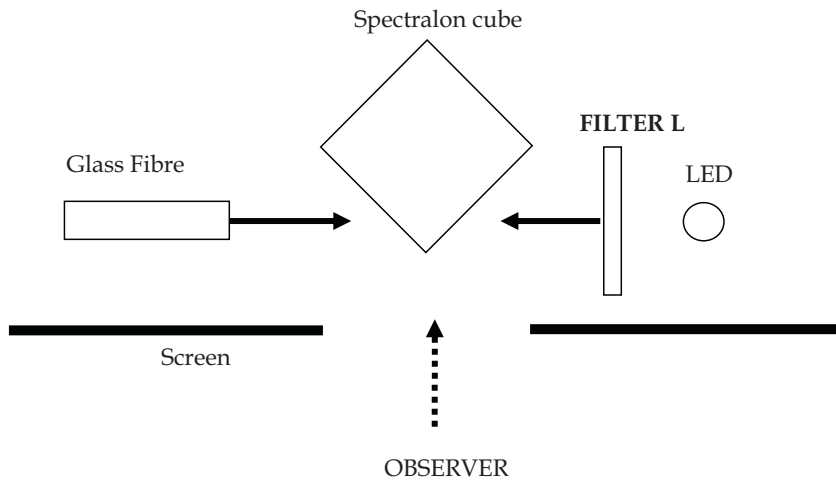
In Colour_Test_1, the radiation guided by glass fibres represented the reference quantity. This glass fibre lighting was compared to the filtered LED emission. Spectral tests on the effect of a set of filters mounted on the LED sources individuated the filter (FILTER_L), which minimised the colour difference. In Colour_Test_2 the filtered LED illumination was considered as the reference. The comparison test was performed for the light guided by plastic fibres and the emission of LED with FILTER_L. The choice of the best filter (FILTER_F) for plastic fibres was made by testing several filters and finding the spectrum approaching the reference one.

The experimental set-up included two channels guiding the two types of radiation to be compared on two faces of a *Spectralon* cube. In front of the *Spectralon* cube a screen with a hole was positioned so that the observer, located at a suitable distance, had a view angle of 2° (*fovea* vision). For balancing the luminance, neutral filters were mounted on the two channel lights, thus facilitating the colour matching by the observer.

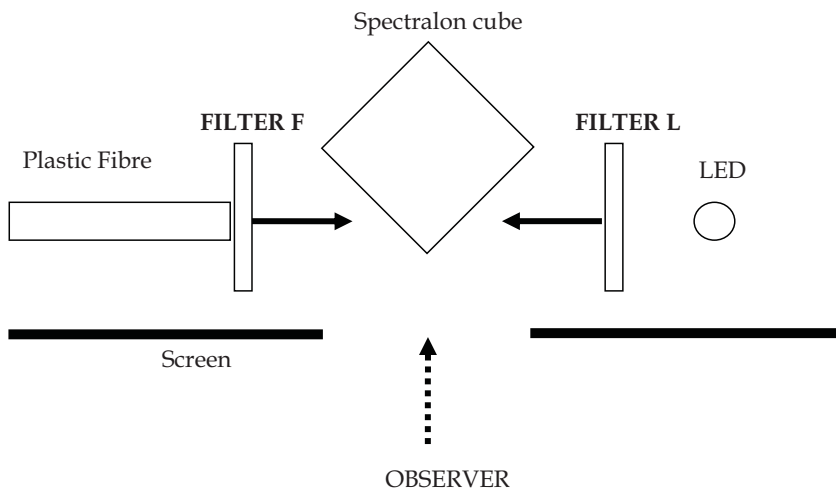
All tests were repeated with several different observers to obtain a preliminary selection of the most suitable filters. Then the final filter choice was made on the basis of the chromatic coordinates measured by the Minolta spectrophotometer CS1000.

The examined quantities were the chromatic coordinate (u',v') and the distance D on the (u',v') diagram: the results for the two colour tests are separately compared in Tables 5a, 5b, 6a and 6b. The criterion for selecting the optimum filter was the minimum distance between reference and filtered light. The (u',v') chromatic coordinates were preferred to the (x,y) coordinates since they appeared to be more linear. The 1976 (u',v') chromaticity diagram is significantly more uniform than the (x,y) diagram, yet it is still far from perfect. In fact in the (u',v') diagram the distance between two colour-points, in a quadratic calculation, is not rigorously correct because indistinguishable colours are included inside ellipses. However, the use of the distance between two colour-points is more correct in the (u',v') -system than in the (x,y) -system [17-18].

For Colour_Test_1, Table 5a examines the colour of LED emission and glass fibre lighting, both measured without filtering. The errors are $< 1\%$ for all quantities in Tables 5 and 6. The preliminary choice of FILTER_L was represented by filters #2 "Bastard Amber" and #304 "Pale Apricot" of the Rosco catalogue. The chromatic coordinates measured after the introduction of the proposed filters are compared in Table 5b, where filter #02 corresponded to the minimum distance on the chromaticity diagram.



(a)



(b)

Fig. 20. (a) Set-up for Colour_Test_1 comparing Glass Fibre and LED lights. (b) Set-up for Colour_Test_2 comparing Plastic Fibre and filtered LED lights.

| | u' | v' | D |
|---------------------|--------|--------|--------|
| Glass Optical Fibre | 0.2206 | 0.5079 | --- |
| LED | 0.2000 | 0.4915 | 0.0263 |

Table 5. (a) Colour_Test_1. Chromatic coordinates $u'v'$ and distance D in the $u'v'$ diagram for the lights before filtering.

| | u' | v' | D |
|---------------------|--------|--------|--------|
| Glass Optical Fibre | 0.2206 | 0.5079 | --- |
| LED + filter #02 | 0.2183 | 0.5083 | 0.0023 |
| LED + filter #304 | 0.2226 | 0.5011 | 0.0071 |

Table 5. (b) Colour_Test_1. Chromatic coordinates $u'v'$ and distance D in the $u'v'$ diagram for the lights after filtering.

| | u' | v' | D |
|-----------------------|--------|--------|--------|
| LED + filter #02 | 0.2168 | 0.5073 | --- |
| Plastic Optical Fibre | 0.1695 | 0.4845 | 0.0525 |

Table 6. (a) - Colour_Test_2. Chromatic coordinates $u'v'$ and distance D in the $u'v'$ diagram for the lights before filtering.

| | u' | v' | D |
|-----------------------------|--------|--------|--------|
| LED + filter #02 | 0.2168 | 0.5073 | --- |
| Plastic Fibre + filter #03 | 0.2064 | 0.5065 | 0.0104 |
| Plastic Fibre + filter #17 | 0.2274 | 0.5205 | 0.0169 |
| Plastic Fibre + filter #317 | 0.2310 | 0.5236 | 0.0216 |

Table 6. (b) - Colour_Test_2. Chromatic coordinates $u'v'$ and distance D in the $u'v'$ diagram for the lights after filtering.

In Colour_Test_2, the light colour was measured with LED with filter #02 and on plastic fibre without a filter: Table 6a shows the results. Three possibilities for FILTER_F were identified in the Rosco catalogue: #3 "Dark Bastard Amber", #17 "Light Flame" and #317 "Apricot". Table 6a compares the chromatic coordinates measured with the possible FILTERS_F and the minimum distance D in the (u',v') diagram corresponded to filter #03.

Combining the results of both colour tests, it can be concluded that the nearest illumination colours were obtained by:

1. Light transmitted by glass optical fibres
2. Emission of LED with filter #02 "Bastard Amber"
3. Light guided by plastic fibres with filter #03 "Dark Bastard Amber"

5.6 Installation and validation of the museum plant demonstrator

A demonstrator of our solar collection system was installed in a prestigious museum in Florence to provide illumination inside several large showcases. The width of the showcases can be 5m or 2m, while the height is 3m. The photos of Fig. 21 present two 5m X 3m showcases: the pictures show the showcases before (left) and after (right) the installation of the solar lighting plant. The installation of the lighting terminations within the showcases was realised in the occasion of a re-styling of the exposition showcases, with displacement



Fig. 21. Two museum showcases without (left) and with (right) the internal lighting supplied by the installed solar plant.

of the shelves and consequent new arrangement of the exhibit items (particularly evident in the lower pictures). The museum plant demonstrator included two separated installations: five devices were placed on the museum roof (Fig. 15a) and four devices were located in the garden. The roof devices were devoted to supply internal illumination in a room of the museum; while the garden installation had didactic purposes.

Each device (in Fig. 14) included eight solar lenses (in Fig. 16), coupled to eight fibre bundles, each of which had seven fibre terminations. The plastic optical fibres transported the light, concentrated by the solar collectors, within the showcases realising the lighting points that are suitably distributed within the spaces to be lighted. The total number of lighting terminations was $5 \times 8 \times 7 = 280$ (from 5 devices with 8 collectors each and 7 terminations in every fibre bundle).

Museum illumination had several fundamental requirements on: illuminance depending on the exhibit items; equivalence between the two lighting types (solar light and LED); light colour and uniformity. Lighting hue and colour balance have been examined in Sect. 5.5, where photometric and colorimetric measurements have determined the appropriate filters for LED emission and light guided by plastic fibres. The museum experts indicated 100 ± 120 lx as average illuminance required to light the showcase interior. This value took into account the illuminance levels recommended by the International Council of Museum [19-20]. The exhibition objects were basically weapons, armatures and metallic objects: items made of metal, stone and ceramic have no limits on maximum illuminance; but some exposed objects were made of leather or wood and others contained horn, bone or ivory and for these materials the illuminance limit is 150 lx. The more fragile exhibit items were costumes and textiles that should not receive illumination higher than 50 lx.

The two lighting configurations, with plastic fibres or LED, were separately estimated and practically experimented directly within the showcases to individuate the best arrangement of the lighting points. The vertical positioning of the lighting spots improved the light uniformity, with respect to the horizontal positioning. The total emission angle was about 120° for LED and around 60° for the plastic fibre (numerical aperture $NA=0.48$) thus the LED lighting achieved a higher distribution inside the showcases. On the other hand, fibre terminations could be orientated to maximise the uniformity of lighting distribution. The selected fibres disposition and LED arrangement fulfilled illuminance correspondence and illuminance level requirements. The illuminance measured on the showcase background resulted to be between 80 lx and 170 lx; the employed luxmeter had an error of $2\% \pm 1$ digit. The solar illuminance within the showcases obviously depended on the external sunlight irradiation, which presented daily and monthly variations. This effect introduced fluctuations in the solar illuminance provided by the fibres, but the illuminance variations were judged compatible with the requirements of museum lighting.

6. References

- [1] Winston R. Light collection within the framework of geometrical optics. *J Opt. Soc. Amer.* 60 (2), 245-247 (1970).
- [2] Winston R, Minano J C, Benitez P. *Non-Imaging Optics. Optics and Photonics*. Elsevier Academic Press USA, 2005.

- [3] Collares - Pereira M, Rabl A, Winston R. *Lens-mirror combinations with maximal concentration*. Applied Optics 16 (10), 2677-2683 (1977).
- [4] Jenkins DG. *High-uniformity solar concentrators for photovoltaic systems*. Proc. SPIE 4446, 52-59, (2001).
- [5] Luque A. *Solar cells and optics for photovoltaic concentration*. The Adam Hilger Series on Optics and Optoelectronics. Bristol and Philadelphia; ISBN 0-85274-106-5; 1989.
- [6] Winston R, Goodman N B, Ignatius R, Wharton L. *Solid-dielectric compound parabolic concentrators: on their use with photovoltaic devices*. Applied Optics 15 (10), 2434-2436 (1976).
- [7] Xiaohui Ning. *Three-dimensional ideal θ_1/θ_2 angular transformer and its uses in fiber optics*. Applied Optics 27 (19), 4126-4130 (1988).
- [8] Cariou J M, Dugas J, Martin L. *Transport of Solar Power with Optical Fibres*. Solar Power 29 (5), 397-406 (1982).
- [9] Liang D, Nunes Y, Monteiro L F, Monteiro M L F, Collares -Pereira M. *200W solar power delivery with optical fiber bundles*. SPIE Vol. 3139, 277-286 (1997).
- [10] Sansoni P, Francini F, Fontani D, Mercatelli L, Jafrancesco D. *Indoor illumination by solar light collectors*. Lighting Res. & Technol. 40 (4), 323-332 (2008).
- [11] *Solar Collectors, Power Storage and Materials*. Edited by Francis de Winter. The MIT press Cambridge, Massachusetts London ISBN 0-262-04104-9; 1991.
- [12] Ciamberlini C, Francini F, Longobardi G, Piattelli M, Sansoni P. *Solar system for the exploitation of the whole collected energy*. Optics and Laser in Engineering 39 (2), 233-246 (2003).
- [13] Fontani D, Francini F, Jafrancesco D, Longobardi G, Sansoni P. *Optical design and development of fibre coupled compact solar collectors*. Lighting Res. & Technol. 39 (1), 17-30 (2007).
- [14] Fontani D, Francini F, Sansoni P. *Optical characterisation of solar collectors*. Optics and Laser in Engineering 45, 351-359 (2007).
- [15] Fontani D, Sansoni P, Francini F, Jafrancesco D, Mercatelli L. *Sensors for sun pointing*. proceedings of WREC/WREN World Renewable Energy Congress / Network 2008, Editor A. Sayigh 2008 WREC, Glasgow - UK, 19-25 July 2008.
- [16] Fontani D, Sansoni P, Francini F, Mercatelli L, Jafrancesco D. *A pinhole camera to track the sun position*. t5.1.O12, ISES Solar World Congress 2007, Beijing - China, 18-21 Sept. 2007.
- [17] Wyszecki G, Stiles W S. *Color Science. Concepts and Methods. Quantitative Data and Formulae*. Second Edition A Wiley-Interscience Publication, John Wiley and Sons Inc, New York; 1982.
- [18] Y. Ohno, *CIE Fundamentals for Color Measurements*, Proc. IS&T NIP16 International Conference on Digital Printing Technologies, Vancouver, Canada, Oct. 15-20 2000: 540-545 (2000).
- [19] Cuttle C. *Damage to museum objects due to light exposure*. Lighting Res. & Technol. 28 (1), 1-10 (1996).
- [20] Castellini C, Cetica M, Farini A, Francini F, Sansoni P. *Dispositivo per il monitoraggio della radiazione ultravioletta e visibile in ambiente museale*. Colorimetria e Beni culturali - SIOF, atti dei convegni Firenze 1999 e Venezia 2000, 168-180 (2000).

- [21] Littlefair P.J. *The luminous efficacy of daylight: a review* Lighting Res. & Technol., 17 (4), 162-182 (1985).
- [22] EERE Information Centre (<http://www1.eere.energy.gov/buildings/ssl/efficacy.html>) of the U.S. Dept. of Energy - Energy Efficiency & Renewable Energy (EERE).



Solar Collectors and Panels, Theory and Applications

Edited by Dr. Reccab Manyala

ISBN 978-953-307-142-8

Hard cover, 444 pages

Publisher Sciyo

Published online 05, October, 2010

Published in print edition October, 2010

This book provides a quick read for experts, researchers as well as novices in the field of solar collectors and panels research, technology, applications, theory and trends in research. It covers the use of solar panels applications in detail, ranging from lighting to use in solar vehicles.

How to reference

In order to correctly reference this scholarly work, feel free to copy and paste the following:

Paola Sansoni, Daniela Fontani, Franco Francini, Luca Mercatelli, David Jafrancesco, Elisa Sani and Debora Ferruzzi (2010). Internal Lighting by Solar Collectors and Optical Fibres, Solar Collectors and Panels, Theory and Applications, Dr. Reccab Manyala (Ed.), ISBN: 978-953-307-142-8, InTech, Available from: <http://www.intechopen.com/books/solar-collectors-and-panels--theory-and-applications/internal-lighting-by-solar-collectors-and-optical-fibres>

INTECH
open science | open minds

InTech Europe

University Campus STeP Ri
Slavka Krautzeka 83/A
51000 Rijeka, Croatia
Phone: +385 (51) 770 447
Fax: +385 (51) 686 166
www.intechopen.com

InTech China

Unit 405, Office Block, Hotel Equatorial Shanghai
No.65, Yan An Road (West), Shanghai, 200040, China
中国上海市延安西路65号上海国际贵都大饭店办公楼405单元
Phone: +86-21-62489820
Fax: +86-21-62489821

© 2010 The Author(s). Licensee IntechOpen. This chapter is distributed under the terms of the [Creative Commons Attribution-NonCommercial-ShareAlike-3.0 License](#), which permits use, distribution and reproduction for non-commercial purposes, provided the original is properly cited and derivative works building on this content are distributed under the same license.